AIMS Mathematics, 11(7): 21069–21090.
DOI: 10.3934/math.2026855
Received: 09 April 2026
Revised: 26 June 2026
Accepted: 03 July 2026
Published: 16 July 2026

https://www.aimspress.com/journal/Math

Research article

Bifurcation analysis and dynamic behavior of a discrete predator–prey system incorporating Allee effects and environmental factors

Abdulaziz Almaslokh[1], **A. A. Elsadany**[1,*], **B. Alreshidi**[1] **and A. S. Zaki**[2]

[1] Department of Mathematics, Faculty of Sciences and Humanities in Al-Kharj, Prince Sattam bin Abdulaziz University, Al-Kharj 11942, Saudi Arabia

[2] Mathematics Department, Faculty of Science, Aswan University, Aswan 81528, Egypt

* **Correspondence:** Email: aelsadany1@yahoo.com.

Abstract: In this paper, we study a discrete-time predator-prey model with a weak Allee effect and multiple environmental factors: Prey refuge, water availability, and moonlight intensity. A major contribution is the biologically inspired synthesis of Allee effects with multiple environmental drivers in a unified discrete-time framework. This class of discrete ecological systems is of considerable theoretical interest due to the possibility of richer dynamics than in their continuous counterparts. The paper provides a detailed study of equilibrium identification, local stability analysis, bifurcation analysis, and numerical simulations. We derive conditions for non-negative equilibria, investigate local stability, and characterize dynamical transitions from stable coexistence to oscillatory and more complex behaviors. In particular, explicit analytical conditions are obtained for the occurrence of two codimension-one bifurcations: The flip (period-doubling) bifurcation, which leads to cycles of period two and higher, and the Neimark–Sacker bifurcation, which gives rise to invariant cycles and quasiperiodic dynamics. A particular strength is the combination of analytical bifurcation arguments with numerical evidence such as bifurcation diagrams, phase portraits, and maximal Lyapunov exponents. The results demonstrate that the synergistic impact of a weak Allee effect threshold, combined with with variables such as prey refuge, water availability, moonlight intensity, and predator interference, significantly enriches the system's dynamic behavior.

Keywords: discrete predator–prey model; stability analysis; environmental factors; codimension-one bifurcation
Mathematics Subject Classification: 37N25, 37N30, 39A28, 39A30

1. Introduction

The Lotka–Volterra predator-prey model is widely recognized as a fundamental framework in population dynamics. The concept of predator-prey interactions was originally formulated independently by Lotka [1] and Volterra [2] in their respective seminal works. Building on their work, Holling [3] proposed more ecologically realistic models by introducing three different types of functional responses to describe how predation behavior varies among species. The functional response is an important component in understanding how predator-prey systems evolve over time. Numerous functional forms have since been incorporated into these models, including Holling type I [4], type II [5, 6], type III [7], type IV [8], ratio-dependent [9], Leslie–Gower [10], and Beddington–DeAngelis types [11]. In recent years, many researchers [12–14] have endorsed discrete-time models governed by difference equations as superior to continuous-time models, particularly for species exhibiting non-overlapping generations. These discrete models not only provide enhanced biological realism but also demonstrate a significantly broader spectrum of complex dynamics, encompassing phenomena such as flip bifurcation, chaos, heteroclinic cycles, and Neimark–Sacker bifurcations. Furthermore, it is widely acknowledged that the mere presence of a predator, rather than predation itself, can substantially impact prey populations by altering their physiology and behavior. Consequently, numerous prey species exhibit a range of anti-predator strategies, including harvesting [15], utilization of refuges [16], and behavioral modifications induced by fear [17], among others.

Mathematical modeling is crucial for analyzing predator-prey dynamics, particularly in assessing the influence of ecological factors on population stability and equilibrium. Among these elements, prey refuges have received increased attention in recent years, with numerous studies investigating their impact within predator-prey systems [18–21]. The Allee effect, which American scientist Allee proposed in 1932, is another crucial part of ecology. It examines how living in groups impacts the growth of a population. Reasonable population densities may enhance survival and reproduction; however, both extremely sparse and overly crowded populations might hinder growth. There are two main varieties of the Allee effect: strong and weak. In strong cases, population growth slows down at low densities, whereas in weak cases, growth continues at low densities. This effect is especially relevant for small populations because it changes how they grow, how likely they are to survive, and how likely they are to go extinct. This is a vital factor to keep in mind when planning conservation and management initiatives (Eva–Chirodeep [22]). In addition to refuges and the Allee effect, additional ecological factors play a significant role in interactions between predators and prey. One such factor is the fear effect, which refers to changes in the behavior of prey caused by the presence of predators, even when there is no direct predation [23, 24]. Furthermore, visual perception is particularly crucial in predator-prey interactions because both predators and prey rely on sight to locate food and dangers. The quantity of moonlight that shines on the Earth changes with the lunar cycle. This can make it harder to see at night, which can make it harder to access shared resources such as water in dry areas and influence how species operate. Many mammals are active at night and depend on visual cues in low light [25]. Changes in the moon's phases that influence nighttime light levels can greatly affect how well they can see and, as a result, how they interact with others and how they survive [26–29].

According to the above discussion, Ashraf Adnan et al. [30] introduced a continuous-time predator–prey model for two mammalian species with Allee effects, prey refuge, water resources,

and moonlight as follows:

$$\begin{aligned}\frac{dx}{dt} &= x\Big(r(1-\frac{x}{k})(\frac{x}{x+A}) - \frac{(a(1-\beta)+\alpha\omega)y}{1+(1-\beta+qm)x}\Big),\\ \frac{dy}{dt} &= y\Big(\frac{\eta(a(1-\beta)+\alpha\omega)x}{1+(1-\beta+qm)x} - \mu\Big),\end{aligned} \tag{1.1}$$

where $x(t)$ and $y(t)$ are the population densities of prey and predator at time t, respectively. The parameter r is the growth rate, and k denotes the carrying capacity in the absence of a mammalian predator. The function $\frac{x}{x+A}$ represents the weak Allee function, where $A > 0$ denotes the Allee level. The functional response is given by $\frac{y(a(1-\beta)+\alpha\omega)}{1+x(1-\beta+qm)}$, where a is the consumption rate, β is the prey refuge rate, ω is the water source availability, m is moonlight, α is an organism's ability to obtain water, and q is the rate at which moonlight becomes brighter or darker. The predator's death rate is denoted by μ, and the conversion rate (conversion efficiency of prey to predator biomass) is denoted by η.

The main novelty is the biological inspiration to combine Allee effects and multiple environmental drivers in a single discrete-time framework. As the system (1.1) has no exact solution, we discretize it using the semi-discretization method, which does not require considering the step size. This is supported by differential equations with piecewise-constant arguments [31–34]. We introduce the model (1.1) in order to derive its discrete approximation. To this end, let $[t]$ be the integer part of t, and consider the average rate of change of the system (1.1) at integer points.

$$\begin{aligned}\frac{1}{x(t)}\frac{dx}{dt} &= \Big(r(1-\frac{x[t]}{k})(\frac{x[t]}{x[t]+A}) - \frac{(a(1-\beta)+\alpha\omega)y[t]}{1+(1-\beta+qm)x[t]}\Big),\\ \frac{1}{y(t)}\frac{dy}{dt} &= \Big(\frac{\eta(a(1-\beta)+\alpha\omega)x[t]}{1+(1-\beta+qm)x[t]} - \mu\Big)\end{aligned} \tag{1.2}$$

with initial conditions $x(0) = x_0 \geq 0,\ y(0) = y_0 \geq 0$.
For $n \leq t < n+1$, the right-hand side of the system (1.2) is constant on each interval $[n, n+1)$. Integrating over this interval gives the discrete-time form:

$$\begin{aligned}x(n+1) &= x(n)exp\Big[r(1-\frac{x(n)}{k})(\frac{x(n)}{x(n)+A}) - \frac{(a(1-\beta)+\alpha\omega)y(n)}{1+(1-\beta+qm)x(n)}\Big],\\ y(n+1) &= y(n)exp\Big[\frac{\eta(a(1-\beta)+\alpha\omega)x(n)}{1+(1-\beta+qm)x(n)} - \mu\Big].\end{aligned} \tag{1.3}$$

The aim of this work is to carry out a complete dynamical analysis of a discrete-time predator-prey model obtained from its continuous-time analog. In particular, the continuous predator-prey model with a weak Allee effect and several environmental parameters, that is, prey refuge, water availability, and moonlight intensity, is transformed into a discrete system using the piecewise constant argument. This study pursues four main objectives under this framework: (i) to determine the conditions for local stability and to find all fixed points of the discrete system; (ii) to apply a lemma from [35, 36] to obtain the necessary conditions for the occurrence of flip and Neimark-Sacker bifurcations; (iii) to analytically prove the existence of codimension-one bifurcations using bifurcation theory and the normal form theorem as given in [37–39]; and (iv) to provide numerical simulations that support and extend the theoretical results, thereby illustrating periodic orbits, invariant cycles, and chaotic attractors.

This paper is structured as follows. We contend that equilibrium points for the model (1.3) exist and are locally stable in Section 2. We discuss the necessary and sufficient conditions for codimension-one bifurcations, such as the flip bifurcation and the Neimark-Sacker bifurcation, in Section 3. Numerical simulations are presented in Section 4 to demonstrate further complicated dynamics and to confirm the theoretical results. In the final Section 5, we offer a concise summary of our mathematical remarks.

2. Existence and stability of fixed points of the model (1.3)

This section discusses the existence of equilibrium points in the system (1.3) and examines their stability by analyzing the eigenvalues of the Jacobian matrix evaluated at the fixed points. The model presented in (1.3) yields three non-negative equilibrium points, as listed below:

1. The trivial fixed point $E_0 = (0,0)$;
2. The semi-trivial fixed point $E_1 = (k,0)$;
3. The interior fixed point $E_2 = (x^*,y^*) = (\frac{\mu}{(1-\beta)(a\eta-\mu)+\eta\alpha\omega-\mu qm}, \frac{rx^*(k-x^*)(1+x^*(1-\beta+qm))}{k(x^*+A)(a-a\beta+\alpha\omega)})$, provided by $\eta > \frac{\mu[1+k(1-\beta+qm)]}{k[(1-\beta)a+\alpha\omega]}$.

To assess the local stability of equilibrium points in the model (1.3), we create a Jacobian matrix and calculate the eigenvalues at each fixed point. The Jacobian matrix at a specific fixed point, $J(x,y)$ is defined as follows:

$$J(x,y) = \begin{pmatrix} a_{11} & a_{12} \\ a_{21} & a_{22} \end{pmatrix}, \tag{2.1}$$

where

$$\begin{cases} a_{11} = \Phi + x\Phi\left[\frac{r(Ak-x^2-2Ax)}{k(x+A)^2} + \frac{y(a-a\beta+\alpha\omega)(1-\beta+qm)}{(1+x(1-\beta+qm))^2}\right], \\ a_{12} = -x\Phi\left[\frac{a-a\beta+\alpha\omega}{1+x(1-\beta+qm)}\right], \\ a_{21} = y\Psi\left[\frac{\eta(a-a\beta+\alpha\omega)}{(1+x(1-\beta+qm))^2}\right], a_{22} = \Psi. \end{cases} \tag{2.2}$$

Also,

$$\begin{cases} \Phi = exp\left[r(1-\frac{x}{k})(\frac{x}{x+A}) - \frac{y(a(1-\beta)+\alpha\omega)}{1+x(1-\beta+qm)}\right], \\ \Psi = exp\left[\frac{\eta x(a(1-\beta)+\alpha\omega)}{1+x(1-\beta+qm)} - \mu\right]. \end{cases} \tag{2.3}$$

Before analyzing the stability of the fixed points of the system (1.3), we recall two fundamental lemmas from Refs. [35–37]. These results provide the necessary and sufficient conditions for classifying the stability behavior of equilibrium points and are presented below for the reader's convenience, as they will be essential to our subsequent stability analysis.

Lemma 1. *[35, 36] Let $F(\lambda) = \lambda^2 + p\lambda + q$. Assume $F(1) > 0$, λ_1 and λ_2 are two roots of $F(\lambda) = 0$. Then,*

1. *$|\lambda_1| < 1$, and $|\lambda_2| < 1$ if and only if $F(-1) > 0$, $q < 1$;*

2. $|\lambda_1| < 1$, *and* $|\lambda_2| > 1$ *(or* $|\lambda_1| > 1$ *and* $|\lambda_2| < 1$*) if and only if* $F(-1) < 0$*;*
3. $|\lambda_1| > 1$, *and* $|\lambda_2| > 1$ *if and only if* $F(-1) > 0$ *and* $q > 1$*;*
4. $\lambda_1 = -1$, *and* $|\lambda_2| \neq 1$ *if and only if* $F(-1) = 0$ *and* $p \neq 0, 2$*;*
5. λ_1, *and* λ_2 *are complex and* $|\lambda_1| = 1$ *and* $|\lambda_2| = 1$ *if and only if* $p^2 - 4q < 0$ *and* $q = 1$.

Lemma 2. *[35,36] Let* $F(\lambda) = \lambda^2 + P\lambda + Q$ *with* $F(1) > 0$*, and let* λ_1, λ_2 *be the two roots of* $F(\lambda) = 0$*. Then the following statements hold:*

1. *It is indicated to as a sink if* $|\lambda_1| < 1$ *and* $|\lambda_2| < 1$ *so the sink is considered to be locally asymptotically stable;*
2. *It is considered a source if* $|\lambda_1| > 1$ *and* $|\lambda_2| > 1$*, so the source is considered to be locally unstable;*
3. *It is considered a saddle if* $|\lambda_1| > 1$ *and* $|\lambda_2| < 1$ *(or* $|\lambda_1| < 1$ *and* $|\lambda_2| > 1$*);*
4. *It is considered non-hyperbolic if either* $|\lambda_1| = 1$ *or* $|\lambda_2| = 1$.

By applying Lemma 2 in the preceding framework, the following theorems concerning the stability of the fixed points E_0 and E_1 are readily obtained.

Theorem 1. *The trivial fixed point* $E_0(0,0)$ *is a non-hyperbolic.*

Proof. The Jacobian matrix at $J(E_0)$ is

$$J(E_0) = \begin{pmatrix} 1 & 0 \\ 0 & exp(-\mu) \end{pmatrix}.$$

According to Lemma 1, we can deduce that $|\lambda_1| = 1$, and $|\lambda_2| \neq 1$. Therefore, E_0 is a non-hyperbolic. This conclusion is based on the fact that the Jacobian matrix $J(E_0)$ has two eigenvalues: $\lambda_1 = 1$ and $\lambda_2 = exp(-\mu)$. □

Theorem 2. *The semi-trivial fixed point* $E_1(k,0)$ *possesses the following characteristics:*

1. *If* $\frac{kr}{k+A} > 1$, *and* $\mu > \frac{k\eta(a-a\beta+\alpha\omega)}{1+k(1-\beta+qm)}$, *then* $|\lambda_{1,2}| < 1$, *and* E_1 *is a locally asymptotically stable;*
2. *If* $\frac{kr}{k+A} < 1$, *and* $\mu > \frac{k\eta(a-a\beta+\alpha\omega)}{1+k(1-\beta+qm)}$, *then* E_1 *is a saddle point where* $|\lambda_1| > 1$, *and* $|\lambda_2| < 1$*;*
3. *If* $\mu = \frac{k\eta(a-a\beta+\alpha\omega)}{1+k(1-\beta+qm)}$, *then* E_1 *is a non-hyperbolic because* $|\lambda_2| = 1$, *and* $|\lambda_1| \neq 1$*;*

Proof. The Jacobian matrix at $J(E_1)$ is

$$J(E_1) = \begin{pmatrix} 1 - \frac{kr}{k+A} & \frac{k(a-a\beta+\alpha\omega)}{1+k(1-\beta+qm)} \\ 0 & exp[\frac{k\eta(a-a\beta+\alpha\omega)}{1+k(1-\beta+qm)} - \mu] \end{pmatrix}.$$

The Jacobian matrix $J(E_1)$ has two eigenvalues, $\lambda_1 = 1 - \frac{kr}{k+A}$, and $\lambda_2 = exp[\frac{k\eta(a-a\beta+\alpha\omega)}{1+k(1-\beta+qm)} - \mu]$. When $\frac{kr}{k+A} > 1$, we get $\lambda_1 < 1$. When $\mu > \frac{k\eta(a-a\beta+\alpha\omega)}{1+k(1-\beta+qm)}$, we have $\lambda_2 < 1$. Furthermore, we conclude $|\lambda_1| < 1$, $|\lambda_1| < 1$, and E_1 implies that locally asymptotically stable. At $\frac{kr}{k+A} < 1$, and $\mu > \frac{k\eta(a-a\beta+\alpha\omega)}{1+k(1-\beta+qm)}$, then $|\lambda_1| > 1$, and $|\lambda_2| < 1$. This implies that E_1 is a non-hyperbolic. When the condition (3) is satisfied, one of the eigenvalues of E_1 is 1, but the other eigenvalue is not equal to 1. This proves that the fixed point E_1 is a location of a transcritical bifurcation at $\mu_{\text{TC}} = \frac{k\eta(a-a\beta+\alpha\omega)}{1+k(1-\beta+qm)}$. Also, when the condition (3) is satisfied, one of the eigenvalues of E_1 is -1, but the other eigenvalue is not equal to -1. This proves that the fixed point E_1 is a location of a flip bifurcation at $r_{FB} = 2(k+A)/k$. □

The following table shows stability and bifurcation behavior associated with the equilibrium point $E_1(k,0)$. The conditions governing the sign of the eigenvalues (or roots of the characteristic equation), the resulting stability status (asymptotically stable, unstable, or non-hyperbolic), and the type of bifurcation (e.g., transcritical, or period-doubling) that may occur as key parameters change are summarized in Table 1.

Table 1. The bifurcation types of $E_1(k,0)$.

Equilibrium	Eigenvalue = 1?	Bifurcation type	Exchange of stability?
$E_0(0,0)$	Yes ($\lambda_1 = 1$)	No bifurcation (isolated, due to Allee structure)	No
$E_1(k,0)$	Yes ($\lambda_2 = 1$ at $\mu = \mu_{\text{TC}}$)	Transcritical bifurcation	Yes (with E_2)
$E_1(k,0)$	Yes ($\lambda_2 = -1$ at $r = r_{FB}$)	Flip bifurcation	Yes (with E_2)

Next, we examine the local dynamical behavior of the system (1.3) in the vicinity of the interior fixed point E_2. To this end, we analyze the system's dynamics within an arbitrarily small open neighborhood of E_2, thereby enabling us to determine whether nearby trajectories converge to, diverge from, or exhibit more complex dynamics around this equilibrium point. The Jacobian matrix evaluated at $E_2(x^*,y^*)$ is expressed as

$$J(x,y) = \begin{pmatrix} 1+x^*\left[\frac{r(Ak-x^{*2}-2Ax^*)}{k(x^*+A)^2} + \frac{y^*(a-a\beta+\alpha\omega)(1-\beta+qm)}{(1+x^*(1-\beta+qm))^2}\right] & -\frac{x^*(a-a\beta+\alpha\omega)}{1+x^*(1-\beta+qm)} \\ \frac{\eta y^*(a-a\beta+\alpha\omega)}{(1+x^*(1-\beta+qm))^2} & 1 \end{pmatrix}.$$

The characteristic equation at this stationary point, which is known as point E_2, can be stated as follows:

$$\lambda^2 + p(x^*,y^*)\lambda + q(x^*,y^*) = 0, \tag{2.4}$$

where

$$\begin{cases} p(x^*,y^*) = -2-G,\ q(x^*,y^*) = 1+G+H, \\ G = x^*\left[\frac{r(Ak-x^{*2}-2Ax^*)}{k(x^*+A)^2} + \frac{y^*(a-a\beta+\alpha\omega)(1-\beta+qm)}{(1+x^*(1-\beta+qm))^2}\right], \\ H = \frac{\eta x^* y^*(a-a\beta+\alpha\omega)^2}{(1+x^*(1-\beta+qm))^3}. \end{cases}$$

By applying Lemmas 1 and 2 to the analysis above, we now examine the stability of the interior equilibrium point by considering the Jacobian matrix of the system (1.3), evaluated at $E_2(x^*,y^*)$. The Jury criterion [35, 36] and the following Lemma 1 will be used to investigate the local stability of the positive fixed point $E_2(x^*,y^*)$. The Jury criterion provides the necessary and sufficient conditions for the fixed point $E_2(x^*,y^*)$ to be locally stable:

$$\begin{aligned} &(i)|p(x^*,y^*)| < 1+q(x^*,y^*), \\ &(ii)q(x^*,y^*) < 1. \end{aligned} \tag{2.5}$$

If the condition (2.5) holds, point $E_2(x^*,y^*)$ is locally asymptotically stable; otherwise, E_2 becomes unstable. Also, if either the condition 4 or the condition 5 of Lemma 1 is met, that is, $F(1) = 1-p+q =$

0; $F(-1) = 1+p+q = 0$; $p^2-4q < 0$; and $q = 1$, then $E_2(x^*, y^*)$ is called non-hyperbolic. We now turn to the analysis of bifurcations that may arise at the interior equilibrium point of the system (1.3). To this end, we employ the framework of bifurcation theory, which enables the detection and characterization of qualitative changes in the dynamical behavior of the system as parameters are varied.

3. Codimension-one bifurcation analysis

From the stability analysis of Section 2, we study the existence of codimension-one bifurcations, that is, the flip bifurcation and the Neimark–Sacker bifurcation, in a neighborhood of the equilibrium point $E_2 = (x^*, y^*)$. We examine the various bifurcation types of the model (1.3) at the fixed point $E_2(x^*, y^*)$, including flip bifurcation and Neimark-Sacker bifurcation, as detailed in Section 2. This study employs the normal form theorem and bifurcation theory, as cited in [37, 38]. Let $u = x - x^*$ and $v = y - y^*$, and define $J(r) = J(x^*, y^*)$. We can translate the fixed point $E_2(x^*, y^*)$ to the origin, thereby reformulating the model (1.3) into

$$\begin{pmatrix} u \\ v \end{pmatrix} \to J(r) \begin{pmatrix} u \\ v \end{pmatrix} + \begin{pmatrix} f_1(u,v,r) \\ f_2(u,v,r) \end{pmatrix}, \tag{3.1}$$

where

$$\begin{cases} f_1(u,v,r) = a_{11}u^2 + a_{12}uv + a_{22}v^2 + a_{111}u^3 + a_{112}u^2v + a_{122}uv^2 + a_{222}v^3 + O(||X||^4), \\ f_2(u,v,r) = b_{11}u^2 + b_{12}uv + b_{22}v^2 + b_{111}u^3 + b_{112}u^2v + b_{122}uv^2 + b_{222}v^3 + O(||X||^4). \end{cases} \tag{3.2}$$

The nonlinear terms $f_1(u,v,r)$ and $f_2(u,v,r)$ are denoted as $F(X)$, where $X = (u,v)^T$. The Taylor expansion about the origin might be articulated as

$$F(X) = \frac{1}{2}B(X,X) + \frac{1}{6}C(X,X,X),$$

where $B(X,X)$ and $C(X,X,X)$ are multilinear mappings. Consequently,

$$\begin{cases} B_1(x,y) = \sum_{j,k=1}^{2} \frac{\partial^2 f_1(\xi,r)}{\partial \xi_j \partial \xi_k} |_{\xi=0}\, x_j y_k = 2a_{11}x_1y_1 + a_{12}(x_1y_2 + x_2y_1), \\ B_2(x,y) = \sum_{j,k=1}^{2} \frac{\partial^2 f_2(\xi,r)}{\partial \xi_j \partial \xi_k} |_{\xi=0}\, x_j y_k = 2b_{11}x_1y_1 + b_{12}(x_1y_2 + x_2y_1), \\ C_1(x,y,z) = \sum_{j,k,l=1}^{2} \frac{\partial^2 f_1(\xi,r)}{\partial \xi_j \partial \xi_k \partial \xi_l} |_{\xi=0}\, x_j y_k z_l = 6a_{111}x_1y_1z_1 + 2a_{112}(x_1y_1z_2 + x_1y_2z_1 + x_2y_1z_1), \\ C_2(x,y,z) = \sum_{j,k,l=1}^{2} \frac{\partial^2 f_2(\xi,r)}{\partial \xi_j \partial \xi_k \partial \xi_l} |_{\xi=0}\, x_j y_k z_l = 6b_{111}x_1y_1z_1 + 2b_{112}(x_1y_1z_2 + x_1y_2z_1 + x_2y_1z_1), \end{cases}$$

$$B(x,y) = \begin{pmatrix} B_1(x,y) \\ B_2(x,y) \end{pmatrix},$$

$$C(x,y,z) = \begin{pmatrix} C_1(x,y,z) \\ C_2(x,y,z) \end{pmatrix}.$$

In the next subsections, we are now able to perform a full examination of the codimension-one bifurcations of the system (1.3) using the above computations. We consider in particular two elementary types of dynamic instabilities: the flip bifurcation (or period-doubling bifurcation) and the Neimark–Sacker bifurcation (or torus bifurcation). For each case, we analyze the critical values of the parameters for which the corresponding bifurcation takes place, verify the transversality conditions, and analyze the resulting changes in the stability and structure of the invariant sets of the system, such as the transition from a stable fixed point to periodic orbits or invariant closed curves.

3.1. Flip bifurcation

The purpose of this part is to study the necessity of a flip bifurcation (period-doubling) at the positive fixed point $E_2(x^*,y^*)$ of the model (1.3). In order to simplify the bifurcation analysis and to concentrate on the role of one parameter only, the study is limited to changes in the parameter r only, whereas all other parameters are considered fixed constants. Consider r as a bifurcation parameter. This implies that $r = \frac{-ky^*(x^*+A)^2(a-a\beta+\alpha\omega)}{2(Ak-2Ax^*-x^{*2})(1+x^*(1-\beta+qm))^3}[2(1-\beta+qm)(1+x^*(1-\beta+qm))+\eta(a-a\beta+\alpha\omega)\Big] - \frac{-2k(x^*+A)^2}{x^*(Ak-2Ax^*-x^{*2})} = r_1$. We are aware that the Jacobian matrix $J(x^*,y^*)$ has a simple eigenvalue $\lambda_1 = -1$ in this instance, whereas the other eigenvalue is $\lambda_2 \neq -1$. The eigenspace E^c is one-dimensional and is spanned by an eigenvector $q \in \mathbb{R}^2$, which satisfies the equation $J(r_1)q = -q$. Furthermore, let $p \in \mathbb{R}^2$ be the adjoint eigenvector, which necessitates that $J^T(r_1)p = -p$. By conducting direct calculations, we can obtain the results associated with these eigenvectors as

$q \sim \Big(b_2+1, -b_1\Big)^T$,

$p \sim \Big(b_2+1, -a_2\Big)^T$.

To normalize p concerning q, we represent it as follows:

$$p = \gamma\Big(b_2+1, -a_2\Big)^T,$$

where a_1, a_2, b_1, and b_2 are the entries of the Jacobian matrix $J(r_1)$ and $\gamma = \frac{1}{(b_2+1)^2+a_2b_1}$.

The scalar product in $\mathbb{R}^2$ is represented by $\langle .,. \rangle$, and it is evident that $\langle p,q \rangle = 1$.

We can certainly state that the map (3.1) is amenable to transformation into its normal form, based on the theories that Kuznetsov offered [37]. This is because the map's limitation to its one-dimensional center manifold at the key parameter value r_1 can be transformed into its normal form:

$$\xi \mapsto -\xi + c(r_1)\xi^3 + O(\xi^4),$$

where

$c(r_1) = \frac{1}{6}\langle p, C(q,q,q)\rangle - \frac{1}{2}\langle p, B(q,(J(r_1)-I)^{-1}B(q,q))\rangle$,

and I represents the identity matrix of dimension 2×2.

Based on the above analysis and the theorems presented in [37–39], we can conclude the following result.

Theorem 3. *If* $r_1 = \frac{-ky^*(x^*+A)^2(a-a\beta+\alpha\omega)}{2(Ak-2Ax^*-x^{*2})(1+x^*(1-\beta+qm))^3}\Big[2(1-\beta+qm)(1+x^*(1-\beta+qm))+\eta(a-a\beta+\alpha\omega)\Big] - \frac{-2k(x^*+A)^2}{x^*(Ak-2Ax^*-x^{*2})}$, *then the model (1.3) undergoes the flip bifurcation at the positive fixed point* $E_2(x^*,y^*)$ *when the parameter* r *varies and passes through* r_1. *Furthermore it, if* $c(r_1) > 0$ *(resp.,* $c(r_1) < 0$*), then the flip bifurcation of the model (1.3) at* $r = r_1$ *is supercritical (resp., subcritical), and the resulting period-2 orbits are stable (resp., unstable).*

3.2. Neimark-Sacker bifurcation

Here, we will explore the fascinating occurrence of the Neimark-Sacker bifurcation, employing insights from the Neimark-Sacker theorems detailed in [37–39] for the map (1.3) at the equilibrium point $E_2(x^*,y^*)$. We will also designate r as the bifurcation parameter, setting $r = \frac{-ky^*(x^*+A)^2(a-a\beta+\alpha\omega)}{(Ak-2Ax^*-x^{*2})(1+x^*(1-\beta+qm))^3}\Big[(1-\beta+qm)(1+x^*(1-\beta+qm))+\eta(a-a\beta+\alpha\omega)\Big] = r_2$. If we follow the formula (2.4), we can describe the eigenvalues of the matrix associated with the linearization of the map (3.1) at the point $(u,v) = (0,0)$ as conjugates with modulus 1.

$$\lambda, \bar{\lambda} = \frac{p(r_2)}{2} \pm \frac{i}{2}\sqrt{4q(r_2) - p^2(r_2)},$$

and $|\lambda|_{r=r_2} = \sqrt{q(0)},\ l = \frac{d|\lambda|}{dr}|_{r=r_2} = \frac{(Akx^*-2Ax^{*2}-x^{*3})}{2\sqrt{1+M}} \neq 0,$
where $M = \frac{x^*y^*(a-a\beta+\alpha\omega)}{(1+x^*(1-\beta+qm))^3}\Big[(1-\beta+qm)(1+x^*(1-\beta+qm))+\eta(a-a\beta+\alpha\omega)\Big]$.
Moreover, it is implies that when $r = r_2$, $\lambda^s, \bar{\lambda}^s \neq 1$, $(s = 1,2,3,4)$, which is equivalent to $p(0) \neq -2,0,1,2$, then, $p(0) \neq -2,2$. Therefore, we only need to require that $p(0) \neq 0,1$, which leads to

$$\mathcal{G} = p(0) + 1 \neq 2,3, \tag{3.3}$$

where $\mathcal{G}$ is the nondegeneracy condition for the bifurcation.

The matrix $J(r)$ has an eigenvalue λ, and the corresponding complex eigenvector q is $\mathbb{C}$. Consequently, $J(r_2)q = \lambda q$, and $J(r_2)\bar{q} = \bar{\lambda}\bar{q}$. In addition, let us assume that the complex eigenvector $p \in \mathbb{C}$ of the transposed matrix $J^T(r)$, which corresponds to the eigenvalue $\bar{\lambda}$, can be defined as

$J^T(r_2)p = \bar{\lambda}p,\ J^T(r_2)\bar{p} = \lambda\bar{p}.$

By doing some simple calculations, we get

$$q \sim \Big(b_2 - \lambda, -b_1\Big)^T,$$

$$p \sim \Big(b_2 - \bar{\lambda}, -a_2\Big)^T.$$

To normalize p relative to q, we define

$$p = \gamma_1\Big(b_2 - \bar{\lambda}, -a_2\Big)^T,$$

where

$$\gamma_1 = \frac{1}{(b_2-\bar{\lambda})^2 + a_2b_1}.$$

Clearly, the scalar product denoted as $\langle .,. \rangle$ in $\mathbb{C}^2$ satisfies the relation $\langle p,q \rangle = 1$. The equivalent

normal form of the restriction of a map (3.1) onto its two-dimensional center manifold, assessed at the crucial parameter value r_2, can be reformed by drawing on the ideas presented by Kuznetsov [37]:

$$z_1 \mapsto \lambda(r_2)z_1(1+d|Z|^2)+O({z_1}^4),$$

where $\lambda(r_2)=e^{i\theta(r_2)}$, $z_1\in\mathbb{Z}^2$, and d is given by the relation

$$c(r_2) = \tfrac{1}{2}e^{-i\theta(r_2)}\Big[\langle p,C(q,q,q)\rangle + 2\langle p,B(q,(I-J(r_2))^{-1}B(q,q))\rangle + \langle p,B(q,(e^{2i\theta(r_2)}I - J(r_2))^{-1}B(q,q))\rangle\Big].$$

By applying the relevant theorems referenced in [37–39], we derive the following conclusions.

Theorem 4. *If the conditions (3.3) are satisfied, and $Re(c(r_2))\neq 0$, a Neimark–Sacker bifurcation occurs at the equilibrium point $E_2(x^*,y^*)$ of the map (1.3) when $r=r_2$. Moreover, the sign of $Re(c(r_2))$ determines the stability of the bifurcating closed invariant curve. Specifically, if $Re(c(r_2))<0$ (resp., $Re(c(r_2))>0$), the resulting closed invariant curve is attracting (resp., repelling) for $r>r_2$ (resp., $r<r_2$).*

In addition to the flip bifurcation at E_1 when $\lambda_2=-1$ (which we already treat), the case $\lambda_2=+1$ at E_1 corresponds to a transcritical bifurcation. Setting $\mu=\mu_{\text{TC}}=\frac{k\eta(a-a\beta+\alpha\omega)}{1+k(1-\beta+qm)}$ yields an eigenvalue $+1$. At this critical value, the boundary equilibrium $E_1(k,0)$ collides with the interior equilibrium $E_2(x^*,y^*)$ and exchanges stability. For $\mu>\mu_{\text{TC}}$, the predator cannot establish itself, and E_1 is stable; for $\mu<\mu_{\text{TC}}$, the interior equilibrium emerges as a sink, and E_1 becomes a saddle. Hence, the model undergoes a transcritical bifurcation at E_1 when the predator's mortality crosses this threshold. Indeed, when μ is larger than this threshold, predators cannot survive, and E_1 is stable; when μ is smaller, the interior equilibrium appears and becomes stable, whereas E_1 loses stability. Regarding $E_0(0,0)$, the eigenvalue $+1$ does not lead to a transcritical bifurcation with any other fixed point, as no equilibrium bifurcates from E_0 under parameter variation. This is because the weak Allee effect term $\frac{A}{x+A}$ vanishes at $x=0$, keeping E_0 isolated.

In the next section, we provide various numerical examples to confirm the theoretical results stated above. The examples are conducted for diverse model parameters, such as varied coefficient values, initial conditions, and key control parameters, to evaluate the robustness and accuracy of the proposed theoretical framework for different configurations.

4. Numerical examples

In this section, we verify the analytical results obtained for the system (1.3). We can enhance our understanding of system functionality through effective analytical and computational methodologies. Bifurcation diagrams illustrate the influence of parameter variations on a system's behavior. This encompasses transitions from stable to chaotic states, periodic orbits, and more complex states such as quasiperiodicity or chaos. Phase portraits, conversely, depict the trajectories, attractors, and the configuration of stable and unstable manifolds inside the system's state space. Maximal Lyapunov exponents (MLEs) for various parameter values quantify the system's sensitivity to initial conditions. This facilitates the distinction between chaotic and regular motion. The inquiry may reveal unexpected

dynamical properties, such as multistability, torus breakdown, intermittency, or aberrant attractors beyond traditional instrumentation. These phenomena enhance our theoretical comprehension and elucidate the functioning of observed complexity, potentially altering our perspective on real-world systems modeled by these dynamics.

Example 1. *Let us set* $k = 10, A = 2, a = 0.2, \beta = 0.4, \alpha = 0.2, \omega = 0.4, q = 0.2, m = 0.02, r = 3$, *and* $\mu = 0.1$ *while varying the parameter* η. *We initiate our numerical simulations using the model's initial values defined as* $E_2(x^*, y^*) = (4.29997, 14.054)$. *Figure 1(a) indicates that a flip bifurcation occurs at* $\eta = 0.358$, *as demonstrated in our theoretical analysis in Section 3. We compute the maximal Lyapunov exponents (MLEs) [36] related to Figure 1(a) and present them in Figure 1(b) to improve our understanding of the system's dynamics. Notably, MLEs are negative for* $\eta > 0.355$, *indicating a stable system. However, we also observe that for* $\eta < 0.355$, *a small proportion of MLEs turn positive. The flip bifurcation, which can be found in Figure 1 at* $\eta = 0.357$, *indicates a critical threshold in the predator's conversion efficiency. Unlike the forward (supercritical) case, this bifurcation is a backward flip bifurcation (subcritical) in nature. Below this threshold (*$\eta < 0.357$*), the predator-prey system shows complex dynamics, with periodic oscillations and chaos, as seen in the bifurcation diagram with its multiple branches and scattered points. At* $\eta = 0.357$, *a subcritical flip bifurcation occurs where an unstable period-*2 *orbit is born from the interior fixed point. Above the threshold (*$\eta > 0.357$*), the system collapses to a stable predator-free state at* $x = 10$, *where predators die out, and prey recover to carrying capacity. This can be clearly seen from Figure 1(a), where for* $\eta > 0.357$, *the prey population settles to a constant value of* $x = 10$, *whereas for* $\eta < 0.357$ *the dynamics are oscillatory or chaotic. This transition is confirmed by the corresponding Lyapunov exponents shown in Figure 1(b), which are positive or near-zero for* $\eta < 0.357$ *(chaos or periodic windows) and negative for* $\eta > 0.357$ *(a stable fixed point). Unlike the forward flip bifurcation, in which a stable period-*2 *orbit emerges smoothly, the backward flip bifurcation generates a region of bistability where the stable interior dynamics (cycles or chaos) coexist with the stable boundary equilibrium for a range of* η *values below the critical point. Biologically, this implies that if the predator conversion efficiency* η *surpasses the critical value* 0.357, *the predator population is doomed to extinction, and the state of coexistence cannot be restored by lowering* η *below the threshold due to the presence of hysteresis. This has important implications for conservation: Managers need to keep predator efficiency* $\eta = 0.357$ *to ensure sustainable coexistence, because approaching the threshold from below risks sudden predator collapse. This figure confirms the analytical predictions of Theorem 3, demonstrating that the interior fixed point loses stability via bifurcations as parameters vary. Thus, Figure 1 shows a subcritical flip bifurcation which results in catastrophic regime shifts instead of smooth transitions, verifying the analytical conditions of Theorem 3 in the subcritical case where the normal form coefficient* $c(\eta_{FB}) > 0$.

Figure 2(a) displays the bifurcation diagram in the (r, x)-plane, where r (the prey growth rate) serves as the bifurcation parameter while η is held fixed. For low values of r ($r < 2.5$), the system possesses a stable interior fixed point, represented by a single thin curve. As r increases through $r \approx 2.5$, a Neimark-Sacker bifurcation occurs, giving rise to quasiperiodic oscillations and invariant cycles, which appear as a thickened band in the diagram. For larger values of r ($r > 3.0$), the system transitions to chaos, characterized by a densely filled band of prey values. It also illustrates the rich dynamical repertoire of the system (1.3), including fixed points, invariant cycles, and chaotic attractors. The basin of attraction in the two-parameter plane (r, η) is illustrated in Figure 2(b). Different colors denote distinct attractors: Blue for the predator-free state E_1, green for the stable interior fixed point,

yellow for limit cycles or quasiperiodic oscillations, and red for chaos. This basin diagram clearly delineates the parameter regions corresponding to each dynamical behavior. The boundary separating the blue region (predator extinction) from the colored regions (coexistence) corresponds precisely to the analytically derived transcritical bifurcation condition, the boundaries between the green, yellow, and red regions correspond to the flip and Neimark-Sacker bifurcation curves predicted by Theorem 3.

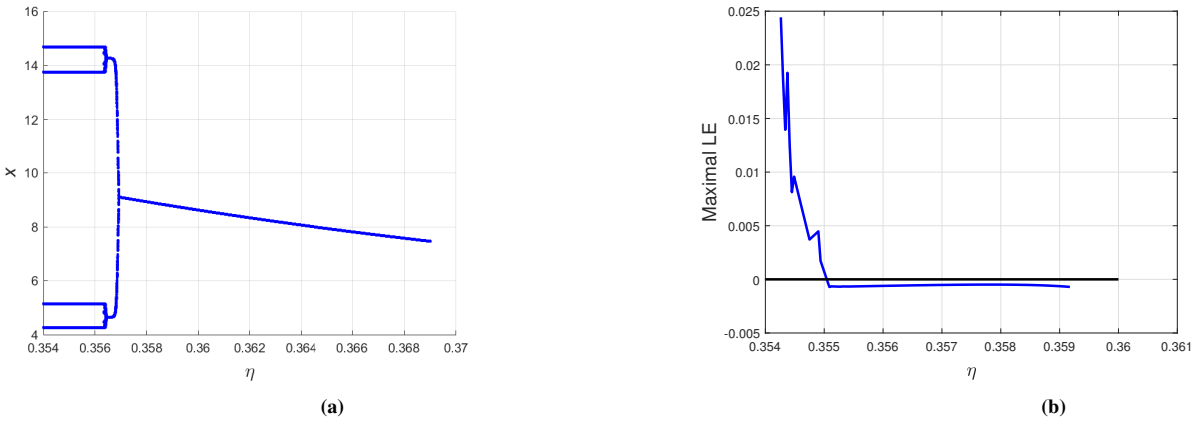

Figure 1. (a) The bifurcation diagram in the (η, x) plane, using parameters $k = 10, A = 2, a = 0.2, \beta = 0.4, \alpha = 0.2, \omega = 0.4, q = 0.2, m = 0.02, r = 3, \mu = 0.1$. illustrates the maximal Lyapunov exponents corresponding to the results in (a) of the model (1.3).

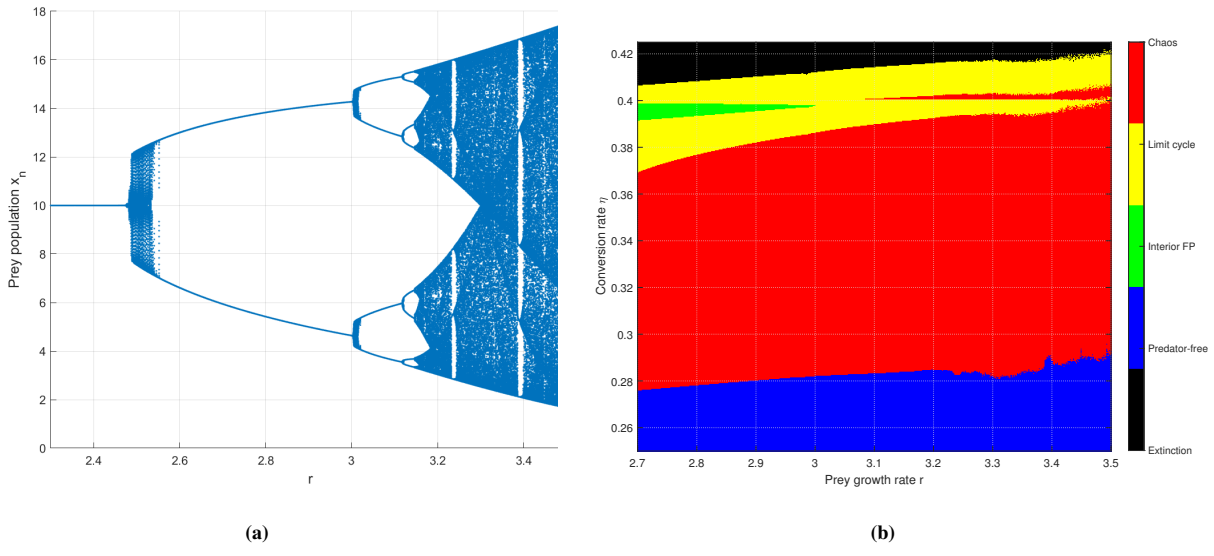

Figure 2. (a) The bifurcation diagram in the (r, x) plane, using parameters $k = 10, A = 2, a = 0.2, \beta = 0.4, \alpha = 0.2, \omega = 0.4, q = 0.2, m = 0.02, \mu = 0.1$. (b) illustrates the basin of attraction of the model (1.3) in the (r, η) plane.

From a biological viewpoint, Figures 1 and 2 collectively demonstrate that the predator-prey

system (1.3) exhibits markedly different behaviors depending on which parameter is varied. Increasing the predator conversion efficiency η above 0.357 causes predator extinction (Figure 1), a catastrophic regime shift from complex coexistence dynamics to a simple predator-free state. Furthermore, because the bifurcation is subcritical (backward bifurcation), hysteresis occurs: Once predators have gone extinct, reducing η back below 0.357 does not necessarily restore the original coexisting state. Consequently, managers must maintain η well below the critical threshold to ensure long-term stability. In contrast, Figure 2(a) demonstrates that increasing the prey growth rate r leads to progressive destabilization via the classical Neimark-Sacker route to invariant cycles and eventually chaos. This represents a distinct ecological scenario: When prey reproduction accelerates, the system becomes oscillatory and unpredictable, yet predators do not necessarily go extinct. Instead, both populations fluctuate irregularly. Figure 2(b) synthesizes these insights by mapping the complete dynamical landscape in the (r,η) parameter space, enabling ecologists to predict which parameter combinations yield stable coexistence (green), periodic cycles (yellow), chaos (red), or predator extinction (blue). The overarching biological implication is clear: To maintain sustainable predator-prey coexistence, managers should keep the predator conversion efficiency η sufficiently low (well below 0.357) and the prey growth rate r within a moderate range (approximately $2.5 < r < 2.7$ for the parameters considered).

Example 2. *Figure 3(a) presents the bifurcation diagram in the (μ,x)-plane, where μ (predator death rate) varies from 0 to 0.25 while other parameters are fixed at $k = 10$, $A = 2$, $a = 0.2$, $\beta = 0.4$, $\alpha = 0.2$, $\omega = 0.4$, $q = 0.2$, $m = 0.02$, $r = 3.3$, and $\eta = 0.32$. For $\mu < 0.09$, the prey population is stable at the carrying capacity, representing the predator-free equilibrium E_1 where low predator mortality allows prey to thrive unchecked. At $\mu \approx 0.09$, a bifurcation occurs, and for $\mu > 0.09$, the system exhibits a dense chaotic band, indicating complex oscillations and chaotic dynamics. This transition reveals that increasing predator death rate beyond the critical threshold destabilizes the system, leading to sustained fluctuations in prey abundance. Biologically, higher predator mortality reduces prey control, allowing prey to escape regulation and undergo complex, unpredictable dynamics. The basin of attraction in the two-parameter plane (μ,η) is depicted in Figure 3(b), where the predator mortality rate μ is varied along the horizontal axis, and the predator attack rate η is varied along the vertical axis. The colors correspond to distinct asymptotic attractors: Blue for the predator-free equilibrium E_1, green for the stable interior fixed point $E_2(x^*,y^*)$, yellow for limit cycles or quasiperiodic oscillations, and red for chaotic attractors. The basin diagram shows four separate dynamical zones. For large values of μ (roughly $\mu > 0.12$), the blue region dominates the parameter space, meaning that the predator cannot establish itself for any assault efficiency, resulting in prey recovery to its carrying capacity. The green zone is a narrow band at low μ ($\mu < 0.08$), and low to moderate η ($\eta \approx 0.3-0.38$), which corresponds to stable predator-prey coexistence. The yellow region is at low μ and higher η ($\eta \approx 0.38-0.44$), corresponding to limit cycle oscillations. The red zone arises at the highest values of η ($\eta > 0.44$) and lowest μ, suggesting chaotic behavior. Theorem 4 analytically predicts that the interior fixed point $E_2(x^*,y^*)$ undergoes a Neimark-Sacker bifurcation when the bifurcation parameter (here η) satisfies $G \neq 2,3$, $Re(c(r_2)) \neq 0$, giving rise to a closed invariant curve. This is confirmed numerically, directly in Figure 3(b). The border between the green region (stable interior fixed point) and the yellow region (limit cycles and quasiperiodic oscillations) exactly matches the Neimark-Sacker bifurcation curve predicted by Theorem 4. When η crosses this limit (for low μ fixed), the system switches from a stable fixed point to quasiperiodic oscillations*

with an invariant closed curve. Furthermore, the lack of chaotic dynamics just outside this boundary, with chaos only occurring at larger values of μ, confirms the supercritical nature of the Neimark-Sacker bifurcation (i.e., $Re(c(r_2)) < 0$), as the bifurcating invariant curve is initially attracting and stable. Figure 3(b) shows good agreement between the analytically obtained bifurcation conditions and the numerically calculated basin borders, which verifies the theoretical framework presented in Section 3.2.

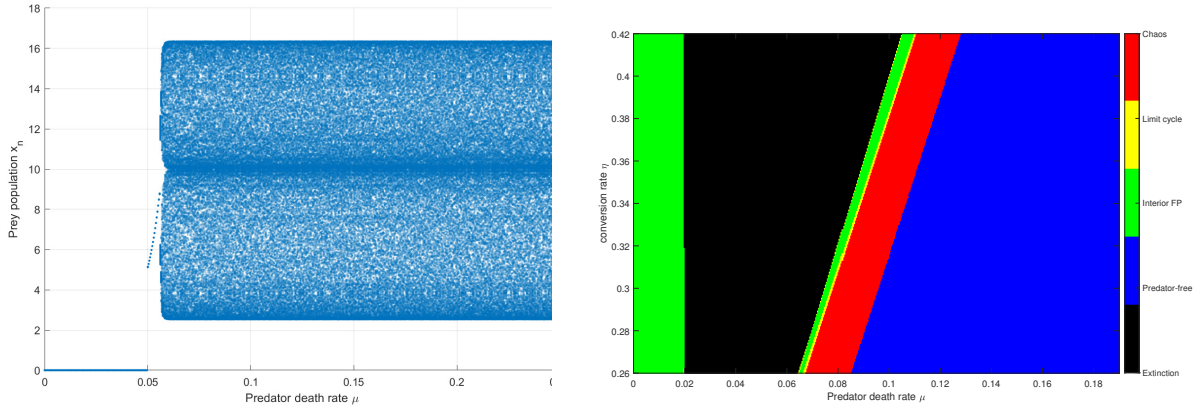

(a) **(b)**

Figure 3. (a) The bifurcation diagram in the (μ, x) plane, using parameters $k = 10, A = 2, a = 0.2, \beta = 0.4, \alpha = 0.2, \omega = 0.4, q = 0.2, m = 0.02, r = 3.3, \mu = 0.1$. (b) illustrates the basin of attraction of the model (1.3) in the (μ, η) plane.

Example 3. *In Figure 4(a-g), the phase portraits of the system (1.3) are given. It gives important insights into the transition from stable dynamics to complicated oscillatory behavior. The subfigures present the plots of a series of dynamical transitions when the key parameters, that is, the predator attack rate η, the prey growth rate r, and the Allee threshold A are varied. For low values of A (e.g., $A = 1.7$, $r = 1.4$, $\eta = 0.4$), the system first shows a stable interior fixed point, corresponding to the sustained coexistence of predator and prey with both populations constant in time. When $A = 1.8$, there is a homoclinic bifurcation, and the dynamics start to get more complicated. At $A = 1.84$, a Neimark–Sacker bifurcation creates an invariant limit cycle from the fixed point E_2, and its radius grows as A increases. Here, we see the start of quasiperiodic oscillations, where the numbers of predator and prey go up and down in a regular but irregular fashion. For $A > 1.86$, the system is temporarily unstable, in that the limit cycle disappears in a heteroclinic bifurcation. For $A > 1.89$, a new closed invariant curve appears around E_2. This curve's amplitude grows again with A, signalling a return to oscillatory dynamics. Finally, the positive maximal Lyapunov exponents indicate that the system enters into a chaotic domain with strange attractor and sensitive dependence to initial conditions for high enough values of parameters ($A = 2$, $r = 4$, $\eta = 0.345$). Biologically, these results show that the Allee threshold A, that is, the minimal population size required for species survival, has two roles: Small increases of A can at first stabilize the predator-prey system by avoiding overexploitation, but then, larger increases destabilize the system, giving rise to periodic cycles, quasiperiodic oscillations, and finally chaos.*

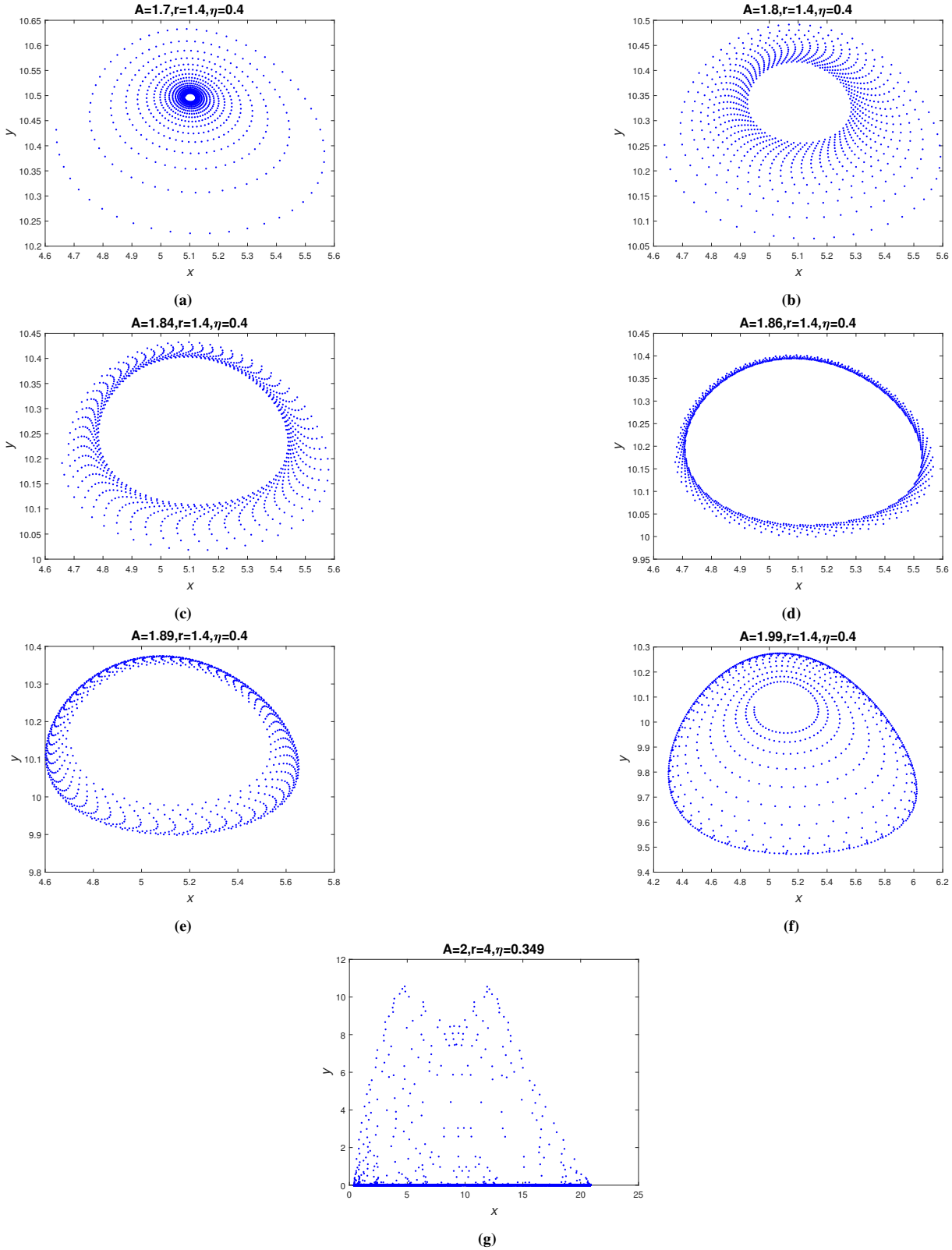

Figure 4. Phase portraits of the model (1.3) near the Neimark–Sacker behavior with different values of A, r, and η.

Example 4. *This example demonstrates the numerical continuation of the positive fixed point* $E_2(x^*,y^*) = (4.29997, 14.054)$. *Parameters are established as* $k = 10$, $A = 2$, $a = 0.2$, $\beta = 0.4$, $\alpha = 0.2$, $\omega = 0.4$, $q = 0.2$, $m = 0.02$, $r = 3$, *and* $\mu = 0.1$, *with* η *designated as a bifurcation parameter. Figure 5 distinctly illustrates that the positive fixed point* E_2 *transitions to instability as a result of a subcritical Neimark-Sacker bifurcation (labeled NS) at* $\eta = 0.399135$. *Furthermore, at* $\eta = 0.357048$, *a subcritical period-doubling bifurcation transpires at* E_2, *denoted as PD. A branch point is also present when* $\eta = 0.352000$, *designated as BP.*

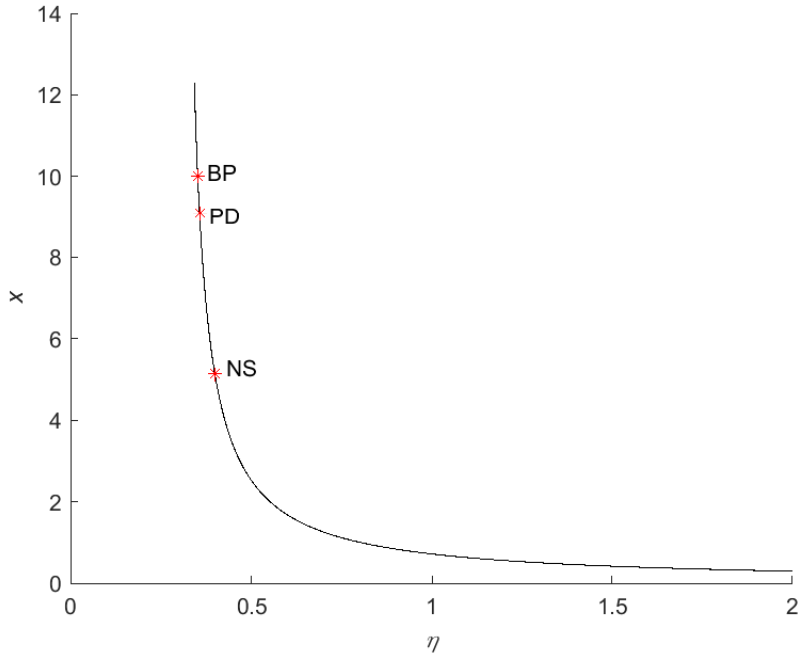

Figure 5. Continuation curve of E^* in (η, x)-plane. The Neimark-Sacker point (NS), period doubling point (PD), and branch point (BP).

The numerical continuation curve of the interior fixed point $E_2^*(x^*,y^*)$ in the (η,x)-plane obtained using the MatContM toolbox is shown in Figure 5. The steady-state prey population x^* is a function of η with other parameters fixed at $k = 10$, $A = 2$, $a = 0.2$, $\beta = 0.4$, $\alpha = 0.2$, $\omega = 0.4$, $q = 0.2$, $m = 0.02$, $r = 3$, and $\mu = 0.1$. The curve contains a number of important bifurcation points. At $\eta \approx 0.352$, a branch point (BP) is created, where E_2^* collides with E_1 via a transcritical bifurcation, the lowest η for predator survival. A period-doubling point (PD) with $\eta \approx 0.357$ occurs where the Jacobian has eigenvalue $\lambda = -1$ satisfies Theorem 3, and the fixed point becomes unstable, and a stable period-2 orbit appears. A Neimark-Sacker point (NS) at $\eta \approx 0.399$ satisfies Theorem 4 with complex conjugate eigenvalues on the unit circle and a closed invariant curve with quasiperiodic oscillations. Biologically, for $\eta < 0.352$, the system converges to the predator-free state E_1. For $0.352 < \eta < 0.357$, the fixed point is stable, corresponding to a sustained coexistence. A subcritical flip bifurcation occurs at $\eta \approx 0.357$ giving rise to a stable period-2 orbit and boom-bust cycles. The system displays periodic or complex dynamics depending on initial conditions for $0.357 \lesssim \eta \lesssim 0.399$. For $\eta \approx 0.399$, a Neimark-Sacker bifurcation leads to quasiperiodic oscillations. Thus, the results of Figure 5 confirm

the correctness of Theorems 3 and 4 and also provide a useful tool to predict dynamical transitions in predator-prey systems.

5. Conclusions

This research has investigated the discrete-time predator-prey model (1.3) considering Allee effects, prey refuge, water resources, and moonlight. We obtained analytical conditions for codimension-one bifurcations: Theorem 3 predicts a flip bifurcation (period-doubling) at the interior fixed point when the prey growth rate r crosses a critical threshold r_1, and Theorem 4 provides conditions for a Neimark-Sacker bifurcation leading to quasiperiodic oscillations on a closed invariant curve. Our theoretical predictions are confirmed by numerical simulations. The subcritical flip bifurcation at $\eta = 0.358$ is shown in Figure 1, where the system collapses from complex dynamics to a predator-free state with hysteresis. The Neimark-Sacker bifurcation in the (r,x)-plane is shown in Figure 2, along with the basin of attraction in the (r,η)-plane that delineates the regions of stable fixed points, limit cycles, chaos, and predator extinction. The supercritical Neimark–Sacker bifurcation is confirmed for $\mu \in [0.09, 0.25]$ in Figure 3, showing the transition from a stable equilibrium to quasiperiodic oscillations. The continuation curve in Figure 5 is used to detect the branch point (BP) at $\eta \approx 0.352$, the period-doubling point (PD) at $\eta \approx 0.357$, and the Neimark–Sacker point (NS) at $\eta \approx 0.399$, which confirms Theorems 3 and 4. Biologically, moderate prey refuge enhances stability, whereas excessive refuge or high predator efficiency triggers oscillations or chaos. Moonlight boosts visibility for both predators and prey, and water sources concentrate prey, increasing predation risk. These results highlight the sensitivity of predator–prey systems to environmental variables and provide practical insights for conservation and management strategies.

Our investigation points to some important contrasts between discrete-time models and their continuous equivalent. Although the continuous model [30] often exhibits smooth transitions to periodic cycles via Hopf bifurcations, our discrete model has a larger dynamical repertoire that includes period-doubling cascades, subcritical flip bifurcations, Neimark-Sacker bifurcations, and deterministic chaos. Unlike continuous systems, where loss of stability usually leads to simple limit cycles, our discrete setting produces sudden regime transitions, bistability, hysteresis, and complicated basin structures. In addition, the discrete formulation reproduces physiologically realistic phenomena such as boom-bust cycles and sensitivity to initial conditions, which are often absent or less evident in continuous formulations. These results suggest that discrete-time modelling is necessary for studying predator-prey systems with non-overlapping generations because pulsed ecological interactions produce dynamics that cannot be reproduced by continuous models.

In future work, we will study codimension-two bifurcations of the model (1.3) including the generalized flip bifurcation and the Chenciner bifurcation leading to multiple invariant cycles and resonance tongues. We will focus on strong resonances (1:2, 1:3, and 1:4) that can lead to period-k orbits, quasiperiodic attractors, heteroclinic cycles, and global bifurcations that change the structure of the basins of attraction. Global analysis will describe the basins, find homoclinic and heteroclinic orbits, and analyze the bistability between several attractors (predator free equilibrium, interior fixed points, limit cycles, and chaos). Understanding these bifurcations is important to predict regime shifts and tipping points in predator-prey systems under environmental changes.

6. Appendix

The expressions of $a_{11}, a_{12}, a_{22}, a_{111}, a_{112}, a_{112}, a_{221}, a_{222}, b_{12}$, and b_{112} are defined as follows:

$$
\begin{cases}
a_{11} = \frac{1}{2}\Big[\Big(\frac{r(Ak-2Ax^*-x^{*2})}{k(x^*+A)^2} + \frac{y^*(a-a\beta+\alpha\omega)(1-\beta+qm)}{(1+x^*(1-\beta+qm))^2}\Big)\Big(1+\frac{rx^*(Ak-2Ax-x^{*2})}{k(x^*+A)^2} + \frac{x^*y^*(a-a\beta+\alpha\omega)(1-\beta+qm)}{(1+x^*(1-\beta+qm))^2}\Big) \\
\quad + \frac{A^2rk-rx^{*3}-4A^2rx^*-Arkx^*}{k(x^*+A)^3} + \frac{y^*(a-a\beta+\alpha\omega)(1-\beta+qm)(1-x^*(1-\beta+qm))}{(1+x^*(1-\beta+qm))^3}\Big], \\
a_{12} = \frac{x^*(a-a\beta+\alpha\omega)(1-\beta+qm)}{(1+x^*(1-\beta+qm))^2} - \big(\frac{a-a\beta+\alpha\omega}{1+x^*(1-\beta+qm)}\big)\big(1+\frac{rx^*(Ak-2Ax-x^{*2})}{k(x^*+A)^2} + \frac{x^*y^*(a-a\beta+\alpha\omega)(1-\beta+qm)}{(1+x^*(1-\beta+qm))^2}\big), \\
a_{22} = \frac{x^*(a-a\beta+\alpha\omega)^2}{2(1+x^*(1-\beta+qm))^2}, \\
a_{111} = \frac{1}{6}\Big[\Big(1+\frac{rx^*(Ak-2Ax-x^{*2})}{k(x^*+A)^2} + \frac{x^*y^*(a-a\beta+\alpha\omega)(1-\beta+qm)}{(1+x^*(1-\beta+qm))^2}\Big)\Big(\big(\frac{r(Ak-2Ax^*-x^{*2})}{k(x^*+A)^2} + \frac{y^*(a-a\beta+\alpha\omega)(1-\beta+qm)}{(1+x^*(1-\beta+qm))^2}\big)^2 \\
\quad + \frac{2Ar(A+k)}{k(x^*+A)^2} - \frac{2y^*(a-a\beta+\alpha\omega)(1-\beta+qm)^2}{(1+x^*(1-\beta+qm))^3}\Big) \\
\quad + \Big(\frac{r(Ak-2Ax^*-x^{*2})}{k(x^*+A)^2} + \frac{y^*(a-a\beta+\alpha\omega)(1-\beta+qm)}{(1+x^*(1-\beta+qm))^2}\Big)\Big(\frac{y^*(a-a\beta+\alpha\omega)(1-\beta+qm)(1-x^*(1-\beta+qm))}{(1+x^*(1-\beta+qm))^2} + \frac{2A^2rk-2Arkx^*-rx^{*3}-3Arx^*}{k(x^*+A)^3} \\
\quad + \frac{8A^2rk-3Arx^{*2}-4A^3r+2Akx^*-4A^2rk}{k(x^*+A)^4} - \frac{y^*(a-a\beta+\alpha\omega)(1-\beta+qm)\big(1+6x^*(1-\beta+qm)^2(1+x^*(1-\beta+qm))\big)}{(1+x^*(1-\beta+qm))^5} \\
\quad - y^*(a-a\beta+\alpha\omega)(1-\beta+qm)^2(1+x^*(1-\beta+qm))^3\Big], \\
a_{112} = \frac{1}{2}\Big[\Big(\frac{(a-a\beta+\alpha\omega)(1-\beta+qm)}{(1+x^*(1-\beta+qm))^2} - \frac{ry^*(Ak-2Ax-x^{*2})(a-a\beta+\alpha\omega)}{k(x^*+A)^2(1+x^*(1-\beta+qm))} - \frac{y^{*2}(a-a\beta+\alpha\omega)^2(1-\beta+qm)}{(1+x^*(1-\beta+qm))^3}\Big)\Big(1+\frac{rx^*(Ak-2Ax-x^{*2})}{k(x^*+A)^2} \\
\quad + \frac{x^*y^*(a-a\beta+\alpha\omega)(1-\beta+qm)}{(1+x^*(1-\beta+qm))^2}\Big) + \frac{rx^*(Ak-2Ax-x^{*2})(a-a\beta+\alpha\omega)(1-\beta+qm)}{k(x^*+A)^2(1+x^*(1-\beta+qm))^2} + \frac{x^*y^*(a-a\beta+\alpha\omega)^2(1-\beta+qm)^2}{(1+x^*(1-\beta+qm))^4} \\
\quad - \frac{y^*(a-a\beta+\alpha\omega)(A^2rk-Arkx^*-rx^{*3}-4A^2rx^*)}{k(x^*+A)^3(1+x^*(1-\beta+qm))} + \frac{(a-a\beta+\alpha\omega)(1-\beta+qm)(1-x^*(1-\beta+qm))}{(1+x^*(1-\beta+qm))^3}\Big], \\
a_{221} = \frac{1}{2}\Big[\frac{rx^*(Ak-2Ax-x^{*2})(a-a\beta+\alpha\omega)^2}{k(x^*+A)^2(1+x^*(1-\beta+qm))^2} + \frac{x^*y^*(a-a\beta+\alpha\omega)^3(1-\beta+qm)}{(1+x^*(1-\beta+qm))^4} + \frac{(a-a\beta+\alpha\omega)^2(1-x^*(1-\beta+qm))}{(1+x^*(1-\beta+qm))^3}\Big], \\
a_{222} = -\frac{x^*y^*(a-a\beta+\alpha\omega)^3}{6(1+x^*(1-\beta+qm))^3},\ b_{11} = -\frac{\eta y^*(a-a\beta+\alpha\omega)(1-\beta+qm)\big(2(1+x^*(1-\beta+qm)+\eta(a-a\beta+\alpha\omega)\big)}{2(1+x^*(1-\beta+qm))^4}, \\
b_{12} = \frac{\eta(a-a\beta+\alpha\omega)}{(1+x^*(1-\beta+qm))^2},\ b_{22} = 0,\ b_{111} = \frac{\eta^2y^*(a-a\beta+\alpha\omega)^2(1-\beta+qm)^2\big(2(1+x^*(1-\beta+qm))+\eta(a-a\beta+\alpha\omega)\big)}{3(1+x^*(1-\beta+qm))^7}, \\
b_{112} = -\frac{\eta(a-a\beta+\alpha\omega)(1-\beta+qm)\big(2(1+x^*(1-\beta+qm))+\eta(a-a\beta+\alpha\omega)\big)}{2(1+x^*(1-\beta+qm))^4},\ b_{221} = 0,\ b_{222} = 0.
\end{cases}
$$

Author contributions

Abdulaziz Almaslokh: Conceptualization, formal analysis, writing-review & editing, critical review, funding; A. A. Elsadany: Methodology, formal analysis, writing-review & editing; B. Alreshidi: Conceptualization, formal analysis, graphics, drawing writing-review & editing, critical review; A. S. Zaki: Conceptualization, formal analysis, graphics, drawing writing-review & editing, critical review. All authors have read and approved the final version of the manuscript for publication.

Use of Generative-AI tools declaration

The authors declare they have not used artificial intelligence (AI) tools in the creation of this article.

Acknowledgments

The authors extend their appreciation to Prince Sattam bin Abdulaziz University for funding this research work through the project number (PSAU/2025/01/37224).

Conflict of interest

The authors declare no conflicts of interest.

References

1. A. J. Lotka, *Elements of mathematical biology*, Williams and Wilkins, Baltimore, 1925.
2. V. Volterra, *Variazioni e fluttuazioni del numero di'individui in specie animali conviventi*, Memoria della Reale Accademia Nazionale dei Lincei, 1926, 31–113.
3. C. S. Holling, *The functional response of predator to prey density and its role in mimicry and population regulation*, The Memoirs of the Entomological Society of Canada 45, 1965, 1–60.
4. S. M. Li, X. L. Wang, X. L. Li, K. L. Wu, Relaxation oscillations for Leslie-type predator–prey model with Holling Type I response functional function, *Appl. Math. Lett.*, **120** (2021), 107328. https://doi.org/10.1016/j.aml.2021.107328
5. M. Lu, J. C. Huang, Global analysis in Bazykin's model with Holling II functional response and predator competition, *J. Differ. Equations*, **280** (2021), 99–138. https://doi.org/10.1016/j.jde.2021.01.025
6. C. F. Arias, G. Bl, M. Falconi, Dynamics of a discrete-time predator–prey system with Holling II functional response, *Qual. Theor. Dyn. Syst.*, **21** (2022), 1–48. https://doi.org/10.1007/s12346-022-00562-5
7. K. Vishwakarma, M. Sen, Influence of Allee effect in prey and hunting cooperation in predator with Holling type-III functional response, *J. Appl. Math. Comput.*, **68** (2022), 249–269. https://doi.org/10.1007/s12190-021-01520-1

8. J. Zhang, J. Su, Bifurcations in a predator-prey model of Leslie-type with simplified Holling type IV functional response, *Int. J. Bifurcation Chaos*, **31** (2021), 2150054. https://doi.org/10.1142/S0218127421500541

9. X. L. Zhuo, F. X. Zhang, Stability for a new discrete ratio dependent predator-prey system, *Qual. Theor. Dyn. Syst.*, **17** (2017), 189–202. https://doi.org/10.1007/s12346-017-0228-1

10. X. Y. Li, Q. Wang, R. J. Han, An impulsive predator–prey system with modified Leslie–Gower functional response and diffusion, *Qual. Theor. Dyn. Syst.*, **78** (2021), 1–20. https://doi.org/10.1007/s12346-021-00517-2

11. G. H. Zhang, W. D. Wang, X. L. Wang, Coexistence states for a diffusive one-prey and two-predators model with B-D functional response, *J. Math. Anal. Appl.*, **387** (2012), 931–948. https://doi.org/10.1016/j.jmaa.2011.09.049

12. Y. P. Lin, Q. Din, M. Rafaqat, A. A. Elsadany, Y. Q. Zeng, Dynamics and chaos control for a discrete-time Lotka–Volterra model, *IEEE Access*, **8** (2020), 126760–126775. https://doi.org/10.1109/ACCESS.2020.3008522

13. S. X. Wu, X. Y. Meng, Dynamics of a delayed predator- prey system with fear effect, herd behavior and disease in the susceptible prey, *AIMS Math.*, **6** (2021), 3654–3685. https://doi.org/10.3934/math.2021218

14. S. Yıldız, Ş. Bilazeroğlu, H. Merdan, Stability and bifurcation analyses of a discrete Lotka-Volterratype predator-prey system with refuge effect, *J. Comput. Appl. Math.*, **422** (2023), 114910. https://doi.org/10.1016/j.cam.2022.114910

15. S. K. Hassan, S. R. Jawad, The effect of mutual interaction and harvesting on food chain model, *Iraqi J. Sci.*, **63** (2022), 2641–2649. https://doi.org/10.24996/ijs.2022.63.6.29

16. O. Francis, T. Aminer, B. Okelo, J. Manyala, Dynamical analysis of prey refuge effects on the stability of Holling type III four-species predator-prey system, *Results Control Opti.*, **14** (2024), 100390. https://doi.org/10.1016/j.rico.2024.100390

17. A. A. Thirthar, S. J. Majeed, K. Shah, T. Abdeljawad, The dynamics of an aquatic ecological model with aggregation, fear and harvesting effects, *AIMS Math.*, **7** (2022), 18532–18552. https://doi.org/10.3934/math.20221018

18. W. Yang, M. Chen, The impact of predator-dependent prey refuge on the dynamics of a Leslie-Gower predator-prey model, *Asian Res. J. Math.*, **19** (2023), 203–211. https://doi.org/10.9734/arjom/2023/v19i11766

19. R. Kumbhakar, S. Jafari, N. Pal, Impacts of predation-driven Allee effect and refuge on the dynamics of a predator-prey model in a parameter plane, *Int. J. Bifurcat. Chaos*, **35** (2025), 2550036. https://doi.org/10.1142/S0218127425500361

20. M. Ahmidi, K. Mokni, M. Ch-Chaoui, Influence of prey harvesting on the dynamics of a prey-predator system: Multi-parameter bifurcation analysis, *Nonlinear Dynam.*, **113** (2025), 31841–31870. https://doi.org/10.1007/s11071-025-11701-3

21. K. Mokni, M. Ch-Chaoui, Resonant bifurcations and complex dynamics in a coupled logistic prey-predator map with proportional immigration, *Chaos*, **36** (2026), 063118. https://doi.org/10.1063/5.0330765

22. E. Muir, M. J. Lajeunesse, A. M. Kramer, The magnitude of Allee effects varies across Allee mechanisms, but not taxonomic groups, *Oikos*, **7** (2024), 1–10. https://doi.org/10.1111/oik.10386

23. Y. Xue, Impact of both-density-dependent fear effect in a Leslie-Gower predator-prey model with Beddington-DeAngelis functional response, *Chaos Soliton. Fract.*, **185** (2025), 115055. https://doi.org/10.1016/j.chaos.2024.115055

24. C. Zhang, The effect of the fear factor on the dynamics of an eco-epidemiological system with standard incidence rate, *Infect. Dis. Model.*, **9** (2024), 128–141. https://doi.org/10.1016/j.idm.2023.12.002

25. J. J. Bennie, J. P. Duffy, R. Inger, K. J. Gaston, Biogeography of time partitioning in mammals, *P. Natl. A. Sci. USA*, **111** (2014), 13727–13732. https://doi.org/10.1073/pnas.1216063110

26. R. T. Botts, A. A. Eppert, T. J. Wiegman, S. R. Blankenship, A. Rodriguez, A. P. Wagner, et al., Does moonlight increase predation risk for elusive mammals in Costa Rica? *Trop. Conserv. Sci.*, **13** (2020), 1–21. https://doi.org/10.1177/1940082920952405

27. P. Taylor, M. Swan, H. Sitters, A. Smith, J. Di Stefano, Small mammals reduce activity during high moon illumination under risk of predation by introduced predators, *Sci. Rep.*, **13** (2023), 105323. https://doi.org/10.1038/s41598-023-37166-1

28. B. T. Boiseau, J. M. Trinidad, R. N. Knight, R. T. Larsen, B. R. McMillan, L. K. Hall, Influence of moonlight on visits to water sources by mammalian predator and prey: A test of competing hypotheses, *Anim. Behav.*, **210** (2024), 139–152. https://doi.org/10.1016/j.anbehav.2024.02.005

29. W. B. Yao, X. Y. Li, Bifurcation difference induced by different discrete methods in a discrete predator-prey model, *J. Nonlinear Model. Anal.*, **4** (2022), 64–79. https://doi.org/10.12150/jnma.2022.64

30. A. A. Thirthar, P. Panja, S. J. Majeed, K. S. Nisar, Dynamic interactions in a two-species model of the mammalian predator–prey system: The influence of Allee effects, prey refuge, water resources, and moonlights, *Part. Differ. Equ. Appl. Math.*, **11** (2024), 100865. https://doi.org/10.1016/j.padiff.2024.100865

31. Y. Q. Liu, X. Y. Li, Dynamics of a discrete predator-prey model with Holling-II functional response, *Int. J. Biomath.*, **14** (2021), 2150068. https://doi.org/10.1142/S1793524521500686

32. R. M. Ruan, X. Li, Complex dynamical properties and chaos control for a discrete modified Leslie-Gower prey-predator system with Holling II functional response, *Adv. Cont. Discr. Mod.*, **2024** (2024), 1–27. https://doi.org/10.1186/s13662-024-03828-1

33. Y. Li, L. Zhou, F. Geng, Dynamics on semi-discrete Mackey-Glass model, *AIMS Math.*, **10** (2025), 2771–2807. https://doi.org/10.3934/math.2025130

34. Z. Wang, R. Ma, X. Li, Multifarious bifurcations in a discrete Gause type predator-prey model with Allee effect and Holling type-III functional response, *Adv. Cont. Discr. Mod.*, **2026** (2026), 1–35. https://doi.org/10.1186/s13662-026-04099-8

35. X. Liu, D. Xiao, Complex dynamic behaviors of a discrete-time predator-prey system, *Chaos Soliton. Fract.*, **32** (2007), 80–94. https://doi.org/10.1016/j.chaos.2005.10.081

36. S. N. Elaydi, *An introduction to difference equations*, Springer, New York, 1996. https://doi.org/10.1007/978-1-4757-9168-6

37. Y. A. Kuznetsov, *Elements of applied bifurcation theory*, 2 Eds., Springer, New York, **112** (1998).

38. S. Winggins, *Introduction to applied nonlinear dynamical systems and chaos*, Springer, New York, 2003.

39. C. Robinson, *Dynamical systems: Stability, symbolic dynamics and chaos*, 2 Eds., CRC Press, Boca Raton, 1999.

AIMS Press